International Journal of Solids and Structures 46 (2009) 3620–3632

Contents lists available at ScienceDirect

International Journal of Solids and Structures

journal homepage: www.elsevier.com/locate/ijsolstr

Wave propagation in transversely isotropic porous piezoelectric materials

Anil K. Vashishth *, Vishakha Gupta

Department of Mathematics, Kurukshetra University, Kurukshetra 136 119, India

ARTICLE INFO

Article history:
Received 26 September 2008
Received in revised form 2 May 2009
Available online 18 June 2009

Keywords:
Anisotropic
Attenuation
Piezoelectric
Phase velocity
Slowness curve
Wave propagation

ABSTRACT

Wave propagation in porous piezoelectric material (PPM), having crystal symmetry 6 mm, is studied analytically. Christoffel equation is derived for the propagation of plane harmonic waves in such a medium. The roots of this equation give four complex wave velocities which can propagate in such materials. The phase velocities of propagation and the attenuation quality factors of all these waves are described in terms of complex wave velocities. Phase velocities and attenuation of the waves in PPM depend on the phase direction. Numerical results are computed for the PPM $BaTiO_3$. The variation of phase velocity and attenuation quality factor with phase direction, porosity and the wave frequency is studied. The effects of anisotropy and piezoelectric coupling are also studied. The phase velocities of two quasi dilatational waves and one quasi shear waves get affected due to piezoelectric coupling while that of type 2 quasi shear wave remain unaffected. The phase velocities of all the four waves show non-dispersive behavior after certain critical high frequency. The phase velocity of all waves decreases with porosity while attenuation of respective waves increases with porosity of the medium. The characteristic curves, including slowness curves, velocity curves, and the attenuation curves, are also studied in this paper.

1. Introduction

Piezoelectric materials have been extensively used as transducers and sensors due to their intrinsic direct and converse piezoelectric effects that take place between electric fields and mechanical deformation. The coupling nature of piezoelectric materials has widespread applications in many branches of science and technology such as electronics, infranics, navigation, mechatronics, and micro-system technology. Piezoelectric materials are acting as very important functional components in sonar projectors, fluid monitors, pulse generators and surface acoustic wave devices. In recent years, piezoelectric materials have been integrated with the structural systems to form a class of smart structures and embedded as layers or fibers into multifunctional composites. Advanced structures with intelligent self-monitoring and self-control capabilities are increasing due to rapid development for smart space systems and micro-electromechanical structures. Piezoelectric materials having electromechanical coupling effects, have found extensive applications in such smart devices. It is the importance of the phenomena of piezoelectricity and hence of piezoelectric material that since the first discovery by Pierre & Jacques Curie, a lot of work have been done and is being done in different fields related to piezoelectric materials, the survey of literature can be found in many related texts and books, we mention a few: Auld, 1973; Ikeda, 1990; Uchino, 1997; Galassi et al., 2000; Arnau, 2004; Yang, 2005; Newnham, 2005; Katzir, 2006; Tichy et al., 2007; Arnau, 2008. A short survey of the piezoelectric wave propagation and resonance were described by Auld (1981).

Both, theoretical and experimental studies on wave propagation in piezoelectric materials have attracted the attention of scientists and engineers during last two decades. Some theoretical ones are listed here. Nayfeh and Chien (1992) made a study on ultrasonic wave interaction with fluid-loaded anisotropic piezoelectric substrates and derived an analytical expression for reflection and transmission coefficients for monoclinic materials. Dispersion relations for propagation of shear waves in piezoelectric "Super lattice-Substrate" structures were analyzed using a formulation of periodic Hamiltonian system (Zinchuk and Podlipenets, 2000). Zinchuk and Podlipenets (2001) obtained dispersion equations for acousto-electric Rayleigh wave in a periodic layer piezoelectric half-space in a study for the 6 mm crystal class. Recognizing the importance of Green's function in areas of applied mathematics and mechanics, Green's functions for transversely isotropic piezoelectric multilayered half-spaces were obtained by Pan and Han (2004, 2005). Li et al. (2006) presented the formulation of the localization factor and localization length in the disordered periodic layered piezoelectric structures by considering the wave propagating in directions normal and tangential to the layers.

The fact, that the piezoelectric composites are used in manufacturing of high-tech components such as ultrasonic transducers and actuators, has shown a large volume of literature on wave propagation in layered piezoelectric composites (Bisegna and Luciano, 1996; Mesquida et al., 1998; Nayfeh et al., 1999; Mesquida et al.,

* Corresponding author.
E-mail address: anil_vashishth@yahoo.co.in (A.K. Vashishth).

0020-7683/$ - see front matter © 2009 Published by Elsevier Ltd.
doi:10.1016/j.ijsolstr.2009.06.011

2001; Qian et al., 2004a,b; Li and Wang, 2005). Recently, Wang and Yuan (2007) investigated, theoretically and experimentally, the propagation characteristics of Lamb waves in composites with emphasis on group velocity and characteristic wave curves. Decoupling of symmetric and anti-symmetric wave modes, by imposing boundary conditions on mid plane and top surface, for symmetric laminates were shown in this paper. An analytical method for wave propagation in piezoelectric cylindrical laminated shells under the large deformation was presented by using Hamiltonian principle (Dong and Wang, 2007). Recently Zakharenko (2007) founds the new solutions for shear horizontal surface acoustic waves in piezoelectric crystals of classes $\bar{4}3m$ and 23.

Despite the significant progress made in enhancing the coupling characteristics between electrical and mechanical properties in piezoelectric materials, monolithic piezoelectric materials generally exhibit limitation such as brittleness. Due to brittleness nature of piezoelectric ceramics and possible defects of impurity, cavities, microvoids, layer separations, inclusions and microcracks, failure of devices take place easily under mechanical or electrical loading. In order to overcome this limitation, material density is reduced through the addition of controlled porosity and resulting porous piezoelectric materials (PPM) are widely used for applications such as low frequency hydrophones, miniature, accelerometers, vibratory sensors and contact microphones. Due to lower acoustic impedance, these materials can be used to improve mismatch of acoustic impedances at the interfaces of medical ultrasonic imaging devices or underwater sonar detectors (Arai et al., 1991; Hayashi et al., 1991; Mizumura et al., 1991). Use of the piezoelectric effect in porous piezoelectric ceramics offers an original method for studying the coupling between electrical, mechanical, permeability, and of course piezoelectric properties of porous systems.

Experimental studies related to properties of porous piezoelectric materials and influence of porosity on its properties have been made by different authors (Xia et al., 2003; Piazza et al., 2005; Huang et al., 2006; Zeng et al., 2006a,b, 2007; Wang et al., 2008). In a study on characterization and microstructure of porous lead zirconate titanate (PZT) ceramics, Praveenkumar et al. (2005) discussed the correlation of porosity with the properties and microstructure. Studies on manufacturing of porous microstructures and the properties of such porous piezoelectric materials were performed (Bowen et al., 2004; Zhang et al., 2007). Gupta and Venkatesh (2006) developed a finite element model to study the effect of porosity on the electromechanical response of piezoelectric materials. A short term microdamage theory for porous transversely isotropic piezoelectric materials was set forth by Khoroshun and Dorodnykh (2003). The method of investigation based on first order reversal curves (FORC) was proposed by Piazza et al. (2006) for describing the role of porosity on the switching properties on Nb-PZT ceramics with anisotropic porosity prepared using lamellar graphite as pore-forming agent. There are some theoretical models (Hashimoto and Yamaguchi, 1986; Banno, 1989a,b; Smith and Auld, 1990; Banno, 1993; Lacour et al., 1994; Gomez et al., 1995; Gomez and Montero, 1996) which provides the elastic, dielectric and piezoelectric coefficients of piezoelectric composites as a function of porosity/(volume concentration) and of the connectivity. Craciun et al. (1998) and Gomez et al. (2000) made an experimental study on wave propagation in porous piezoceramics.

Although a lot of experimental work has been done on porous piezoelectric ceramics, but work on theoretical studies of wave propagation in such materials is rarely found. On the basis of Biot's theory and strain energy density function, the constitutive equations for PPM were derived (Vashishth and Gupta, 2009). In the present paper, we study the wave propagation in a transversely isotropic porous piezoelectric material. In the Section 2, the basic equations of motion and constitutive equations for porous piezoelectric material were first formulated and then Christoffel equation is derived by making use of those equations. The roots of this equation give the different wave velocities which further define the phase velocity and attenuation quality factor of waves propagating in medium. The numerical computations of the analytical solutions, derived in the Section 2, were done and the results are discussed in the Section 3. In this section, the effects of wave frequency, porosity of the material, piezoelectric interaction and the anisotropy on the phase velocities and attenuation quality factors of four waves are studied. Slowness surfaces and velocity surfaces of these waves are also analyzed in the present paper.

2. Basic equations and their solutions

The equations of motion for a fluid-saturated porous piezoelectric medium, in the absence of body forces, are

$$\begin{aligned}
&\sigma_{ij,j} = \rho_{ij}^{11}\ddot{u}_j + \rho_{ij}^{12}\ddot{U}_j^* + b_{ij}(\dot{u}_j - \dot{U}_j^*),\\
&\sigma_{,i}^* = \rho_{ij}^{12}\ddot{u}_j + \rho_{ij}^{22}\ddot{U}_j^* - b_{ij}(\dot{u}_j - \dot{U}_j^*),\\
&D_{i,i} = 0,\\
&D_{i,i}^* = 0,
\end{aligned} \qquad (i,j = 1,2,3). \tag{1}$$

where σ_{ij}/σ^* are the stress components acting on solid/fluid phase of porous aggregate. The quantities with superscript (*) are associated to the fluid phase of the porous bulk material. u_i/U_i^* are the components of mechanical displacement for solid/fluid phase of porous aggregate. $\boldsymbol{\rho}_{11}(\rho_{ij}^{11})$, $\boldsymbol{\rho}_{12}(\rho_{ij}^{12})$ and $\boldsymbol{\rho}_{22}(\rho_{ij}^{22})$ are dynamical coefficients which depend upon the porosity (f), density of porous aggregate (ρ), pore fluid density (ρ_f) and the inertial coupling parameters. The dissipation function $\mathbf{b}(b_{ij})$ steers the effect of wave frequency (υ), fluid viscosity (μ), solid-matrix permeability $\boldsymbol{\chi}(\chi_{ij})$ and the porosity.

In case of isotropic medium, $b_{ij} = b\delta_{ij}$. The coefficient b (Biot, 1956) is related to Darcy's coefficients of permeability χ by

$$b = \frac{\mu f^2}{\chi}. \tag{2}$$

This dissipation function $\mathbf{b}(b_{ij})$, for anisotropic porous medium, in low frequency range can be written as

$$b_{ij} = f^2\mu[\chi_{ij}]^{-1}. \tag{3}$$

For high frequency range, a boundary layer develops and viscous forces are then confined to this layer and the micro-velocity field in the major portion of the fluid is determined by potential flow (Biot, 1962). The friction force of the fluid on the solid becomes out of phase with relative rate of flow and exhibits a frequency dependence represented by a complex quantity $F(\kappa)$. The complex viscosity function $F(\kappa)$ may be defined by considering oscillatory flow through a slit or a circular pipe and is given by

$$\begin{aligned}
&F(\kappa) = \frac{1}{3}\frac{\sqrt{\imath}\kappa\tanh(\sqrt{\imath}\kappa)}{(1-\tanh(\sqrt{\imath}\kappa)/\sqrt{\imath}\kappa)},\\
&\text{and } \kappa = \sqrt{6\pi}\sqrt{\chi_0\upsilon\rho_f/\mu f}.
\end{aligned} \tag{4}$$

where χ_0 is the norm of the permeability matrix. However, Johnson et al. (1987) presented a viscosity correction factor which describes the transition behavior from viscosity dominates flow in the low frequency range towards inertial dominated flow at the HFR.

The electric enthalpy density function (W^*) for porous piezoelectric material is defined as

$$W^* = \frac{1}{2}[\sigma_{ij}\varepsilon_{ij} + \sigma^*\varepsilon^* - E_iD_i - E_i^*D_i^*], \tag{5}$$

where $\varepsilon_{ij}/\varepsilon^*$ are strain tensor components for solid/fluid phase, respectively. E_i/E_i^* and D_i/D_i^* are electric field and electric

displacement components for solid/fluid phase of porous bulk material, respectively.

This enthalpy density function W^* is a quadratic function of ε_{ij}, ε^*, E_i and E_i^*.

$$W^* = \frac{1}{2}c_{ijkl}\varepsilon_{ij}\varepsilon_{kl} + \frac{1}{2}R\varepsilon^*\varepsilon^* + m_{ij}\varepsilon_{ij}\varepsilon^* - e_{kij}E_k\varepsilon_{ij} - \zeta_{kij}E_k^*\varepsilon_{ij} - \tilde{\zeta}_i E_i\varepsilon^* - e_i^*E_i^*\varepsilon^* - \frac{1}{2}\xi_{ij}E_iE_j - \frac{1}{2}\xi_{ij}^*E_i^*E_j^* - A_{ij}E_iE_j^*, \tag{6}$$

where coefficients $c_{ijkl}/e_{kij}, \zeta_{kij}/m_{ij}, \xi_{ij}, \xi_{ij}^*, A_{ij}/e_i^*, \tilde{\zeta}_i$ and R are tensors of order 4/3/2/1 and zero, respectively.

It is known from the definition of the electric enthalpy density function that

$$\frac{\partial W}{\partial \varepsilon_{ij}} = \sigma_{ij}, \quad \frac{\partial W}{\partial \varepsilon^*} = \sigma^*, \quad \frac{\partial W}{\partial E_i} = -D_i, \quad \frac{\partial W}{\partial E_i^*} = -D_i^*. \tag{7}$$

Eqs. (6) and (7) leads to

$$\begin{aligned}
\sigma_{ij} &= c_{ijkl}\varepsilon_{kl} + m_{ij}\varepsilon^* - e_{kij}E_k - \zeta_{kij}E_k^*,\\
\sigma^* &= m_{ij}\varepsilon_{ij} + R\varepsilon^* - \tilde{\zeta}_k E_k - e_k^*E_k^*,\\
D_i &= e_{ikl}\varepsilon_{kl} + \tilde{\zeta}_i\varepsilon^* + \xi_{il}E_l + A_{il}E_l^*,\\
D_i^* &= \zeta_{ikl}\varepsilon_{kl} + e_i^*\varepsilon^* + A_{il}E_l + \xi_{il}^*E_l^*.
\end{aligned} \tag{8}$$

These are constitutive equations for anisotropic porous piezoelectric materials. c_{ijkl} are elastic stiffness constants. The elastic constant R measures the pressure to be exerted on fluid to push its unit volume into the porous matrix. $e_{kij}/e_i^*, \xi_{ij}/\xi_{ij}^*$ are piezoelectric and dielectric constants for solid/fluid phase, respectively. $m_{ij}; \zeta_{kij}, \tilde{\zeta}_i; A_{ij}$ are the parameters which take into account the elastic; piezoelectric; dielectric coupling between the two phases of the porous aggregate. Further,

$$\varepsilon_{ij} = \frac{1}{2}(u_{i,j} + u_{j,i}), \quad \varepsilon^* = U_{k,k}^*, \quad E_i = -\phi_{,i}, \quad E_i^* = -\phi_{,i}^*, \tag{9}$$

where ϕ and ϕ^* are electric potential functions for solid and fluid phase of the porous aggregate.

The constitutive equations for transversely isotropic porous piezoelectric materials can be written as follows:

To find the harmonic solution of (1) for the propagation of plane waves, let us assume that

$$\begin{aligned}
u_j &= B_j\exp(\iota\omega(p_kx_k - t)),\\
U_j^* &= F_j\exp(\iota\omega(p_kx_k - t)),\\
\phi &= G\exp(\iota\omega(p_kx_k - t)),\\
\phi^* &= H\exp(\iota\omega(p_kx_k - t)),
\end{aligned} \tag{11}$$

where p_k are the components of slowness vector ($\mathbf{p}$) and $\iota^2 = -1$. These can be written as $p_k = n_k/v$ in term of phase velocity (v). The vector $\mathbf{n} = [n_1 \quad n_2 \quad n_3]$ defines the phase direction of wave propagating in a medium. ω is the circular frequency of waves. The direction of phase propagation ($\mathbf{n}$) can be written as

$$n_1 = \sin\theta\cos\varphi, \quad n_2 = \sin\theta\sin\varphi, \quad n_3 = \cos\theta, \tag{12}$$

where θ is the angle made by direction of propagation with the axis of symmetry and φ is the azimuthal angle.

Making use of Eqs. (8)–(11) in Eq. (1), we obtain a system of equations in unknowns B_j, F_j $(j = 1, 2, 3)$, G and H. This system can be reduced into a system which can be written as

$$\begin{aligned}
&\mathbf{A}_1\mathbf{B} + \mathbf{A}_2\mathbf{F} = \mathbf{0},\\
&\mathbf{A}_3\mathbf{B} + \mathbf{A}_4\mathbf{F} = \mathbf{0},\\
&\text{where } \mathbf{B} = \begin{bmatrix} B_1\\ B_2\\ B_3\end{bmatrix}, \quad \mathbf{F} = \begin{bmatrix} F_1\\ F_2\\ F_3\end{bmatrix}.
\end{aligned} \tag{13}$$

The system (13) can be expressed as

$$\mathbf{WB} = \mathbf{0}, \tag{14}$$

where

$$\mathbf{W} = \mathbf{A}_1 - \mathbf{A}_2\mathbf{A}_4^{-1}\mathbf{A}_3. \tag{15}$$

The matrices $\mathbf{A}_1$, $\mathbf{A}_2$, $\mathbf{A}_3$, $\mathbf{A}_4$ and $\mathbf{W}$ and other expressions in these are given in Appendix A.

For simplification, we can write

$$\mathbf{W} = \mathbf{B}h + \mathbf{C} + \frac{\mathbf{D}}{x}, \tag{16}$$

where $h = R/(\rho v^2)$.

$\mathbf{B}$, $\mathbf{C}$, $\mathbf{D}$ and x are given in Appendix B.

The system (14) has a non-trivial solution if

$$\det(\mathbf{W}) = 0. \tag{17}$$

$$\begin{bmatrix}\sigma_1\\ \sigma_2\\ \sigma_3\\ \sigma_4\\ \sigma_5\\ \sigma_6\\ \sigma^*\\ D_1\\ D_2\\ D_3\\ D_1^*\\ D_2^*\\ D_3^*\end{bmatrix} = \begin{bmatrix} c_{11} & c_{12} & c_{13} & 0 & 0 & 0 & m_{11} & 0 & 0 & -e_{31} & 0 & 0 & -\zeta_{31}\\ c_{12} & c_{11} & c_{13} & 0 & 0 & 0 & m_{11} & 0 & 0 & -e_{31} & 0 & 0 & -\zeta_{31}\\ c_{13} & c_{13} & c_{33} & 0 & 0 & 0 & m_{33} & 0 & 0 & -e_{33} & 0 & 0 & -\zeta_{33}\\ 0 & 0 & 0 & c_{44} & 0 & 0 & 0 & 0 & -e_{15} & 0 & 0 & -\zeta_{15} & 0\\ 0 & 0 & 0 & 0 & c_{44} & 0 & 0 & -e_{15} & 0 & 0 & -\zeta_{15} & 0 & 0\\ 0 & 0 & 0 & 0 & 0 & (c_{11}-c_{12})/2 & 0 & 0 & 0 & 0 & 0 & 0 & 0\\ m_{11} & m_{11} & m_{33} & 0 & 0 & 0 & R & 0 & 0 & -\tilde{\zeta}_3 & 0 & 0 & -e_3^*\\ 0 & 0 & 0 & 0 & e_{15} & 0 & 0 & \xi_{11} & 0 & 0 & A_{11} & 0 & 0\\ 0 & 0 & 0 & e_{15} & 0 & 0 & 0 & 0 & \xi_{11} & 0 & 0 & A_{11} & 0\\ e_{31} & e_{31} & e_{33} & 0 & 0 & 0 & \tilde{\zeta}_3 & 0 & 0 & \xi_{33} & 0 & 0 & A_{33}\\ 0 & 0 & 0 & 0 & \zeta_{15} & 0 & 0 & A_{11} & 0 & 0 & \xi_{11}^* & 0 & 0\\ 0 & 0 & 0 & \zeta_{15} & 0 & 0 & 0 & 0 & A_{11} & 0 & 0 & \xi_{11}^* & 0\\ \zeta_{31} & \zeta_{31} & \zeta_{33} & 0 & 0 & 0 & e_3^* & 0 & 0 & A_{33} & 0 & 0 & \xi_{33}^*\end{bmatrix}\begin{bmatrix}\varepsilon_1\\ \varepsilon_2\\ \varepsilon_3\\ 2\varepsilon_4\\ 2\varepsilon_5\\ 2\varepsilon_6\\ \varepsilon^*\\ E_1\\ E_2\\ E_3\\ E_1^*\\ E_2^*\\ E_3^*\end{bmatrix} \tag{10}$$

This leads to

$$(c_1T_1)h^4 + (c_2T_1 + c_1T_2)h^3 + (c_2T_2 + c_1T_3 + T_5)h^2 + (c_2T_3 + c_1T_4 + T_6)h + c_2T_4 + T_7 = 0, \quad (18)$$

where c_1 and c_2 are given in Appendix B and the coefficients $T_1, T_2, T_3, T_4, T_5, T_6, T_7$ are given in Appendix C.

On solving Eq. (18), we obtain four complex roots h_j $(j = 1, 2, 3, 4)$. Corresponding to these four complex roots, we get four complex wave velocities V_j of four waves. The phase velocity and attenuation quality factor for these waves are defined to be

$$v_j = ((V_j)_R^2 + (V_j)_I^2)/(V_j)_R,$$
$$Q_j^{-1} = -2(V_j)_I/(V_j)_R,$$

where

$$V_j = (V_j)_R + \imath(V_j)_I \quad (j = 1, 2, 3, 4). \quad (19)$$

Thus we obtain four plane harmonic waves propagating along a given phase direction in transversely isotropic (6 mm) porous piezoelectric material. The wave with largest phase velocity is termed as stiffened quasi P_1 wave and the wave with smallest phase velocity is termed as stiffened quasi P_2 wave. The other two waves are termed as stiffened quasi S_1 and quasi S_2 waves. The phase velocity of S_2 wave is not affected by piezoelectric effect while that of S_1 wave get affected. Due to this reason S_1 and S_2 waves may be termed as piezoelectric stiffened shear wave and quasi shear wave.

Corresponding to the each value h_j, the solution of homogeneous system (14) defines the polarization vector of the corresponding wave. The skewing angle (angle of deviation) of normalized polarization direction ($\hat{\mathbf{B}}^j$) corresponding to *jth* wave from the direction of propagation ($\mathbf{n}$) is defined as

$$\gamma_j = \cos^{-1}(\hat{\mathbf{B}}^j \cdot \mathbf{n}) \quad (j = 1, 2, 3, 4). \quad (20)$$

Here $j = 1$, 2, 3 and 4 corresponds to P_1, P_2, S_1 and S_2 wave.

3. Numerical results and discussion

In the previous section, a general mathematical model for wave propagation in fluid saturated porous piezoelectric materials was presented. The analytical expressions of phase velocity of propagation and attenuation quality factor of stiffened quasi P_1, P_2 and S_1, S_2 waves, derived in that section, are computed numerically for a particular model. For the purpose of numerical computation we consider a porous piezoelectric material as transversely isotropic (6 mm) $BaTiO_3$ crystal. Following Rasolofasaon and Zinszner (2002), Gupta and Venkatesh (2006) and Hsu and Wu (2008), the elastic, piezoelectric and dielectric constants are given in Tables 1 and 2 and the dynamical coefficients and other parameters, used in the study, are given in Table 3. We have used the data given in Tables 1 and 3 for the purpose of numerical computation unless mentioned specifically.

Table 1
Elastic constants, piezoelectric constants and dielectric constants of $BaTiO_3$ crystal.

Elastic constants (GPa)	Piezoelectric constants (C/m^2)	Dielectric constants (nC/Vm)
$c_{11} = 150.4$	$e_{15} = 11.4$	$\xi_{11} = 10.8$
$c_{12} = 65.63$	$e_{31} = -4.32$	$\xi_{33} = 13.1$
$c_{13} = 65.94$	$e_{33} = 17.4$	$\xi_{11}^* = 11.8$
$c_{33} = 145.5$	$\zeta_{15} = 4.56$	$\xi_{33}^* = 13.9$
$c_{44} = 43.86$	$\zeta_{31} = -1.728$	$A_{11} = 12.8$
$m_{11} = 8.8$	$\zeta_{33} = 6.96$	$A_{33} = 15.1$
$m_{33} = 5.2$	$e_3^* = -3.6$	
$R = 20$	$\tilde{\zeta}_3 = -7.5$	

Table 2
Elastic constants, piezoelectric constants and dielectric constants of $BaTiO_3$ crystal with epoxy.

$\zeta_{15} = \zeta_{31} = \zeta_{33} = e_3^* = 0,\ \xi_{11}^* = 0.038,\ \xi_{33}^* = 0.049,\ A_{11} = 0.018,\ A_{33} = 0.015$
Rest of the values are same as in Table 1

Table 3
Non-dimensional dynamical coefficients, permeability tensor and other parameters.

Dynamical coefficients (non-dimensional)	Permeability tensor (m^2)	Parameters
$[\rho_{11}]_{11} = 0.66$	$\chi_{11} = 1 \times 10^{-10}$	ρ (kg/m^3) $= 5700$
$[\rho_{11}]_{33} = 0.68$	$\chi_{33} = 0.8 \times 10^{-10}$	ρ_f (kg/m^3) $= 1000$
$[\rho_{12}]_{11} = -0.15$		μ (N s/m^2) $= 1 \times 10^{-3}$
$[\rho_{12}]_{33} = -0.13$		υ (Hz) $= 50$ in LFR
$[\rho_{22}]_{11} = 0.64$		υ (Hz) $= 10,000$ in HFR
$[\rho_{22}]_{33} = 0.66$		$\theta = 30^\circ$
		$\varphi = 60^\circ$
		$f = 0.2$

3.1. Evolution of phase velocity and attenuation quality factors with frequency and porosity

In this section, the effects of frequency and porosity on the phase velocities and attenuation quality factors of waves propagating in the medium are discussed. The values of dielectric and piezoelectric constants, etc. are taken zeros, as shown in Table 4, in the non-piezoelectric case.

The numerical computation has been done for the following three data sets:

Set 1 = The values of the elastic, piezoelectric, dielectric and dynamic coefficients as given in Tables 1 and 3 for PPM; represented by dotted curves.
Set 2 = The values of the elastic and dynamic coefficients as given in Tables 4 and 3 for non-piezoelectric porous materials; represented by solid curves.
Set 3 = The values of the elastic, piezoelectric, dielectric and dynamic coefficients as given in Tables 2 and 3 for PPM; represented by dashed curves.

The dependence of phase velocities of P_1 wave (v_1), P_2 wave (v_2), S_1 wave (v_3) and S_2 wave (v_4) on frequency is described in Fig. 1. In this figure and in Figs. 2–4, the results for the data given in Set 1 and Set 3 are represented by dotted and dashed curves, respectively, with scale of y-axis as shown on the left side and those corresponding to the data given in Set 2 are represented by solid curves with scale of y-axis as shown on the right side of the respective graph. The results are computed both for low and high frequency waves. It is a known fact that in low frequency range (LFR), the pore fluid viscosity dominates while inertial terms dominate in the high frequency range (HFR). It is observed that wave velocities increase in LFR but decrease with increase of frequency in HFR. The phase velocity of respective waves in HFR is greater than that in LFR. It can be seen from Fig. 1(b) that after frequency = 0.5 MHz, the phase velocity of all the waves become almost constant, i.e. waves with negligible dispersion. Comparison of dashed and solid curves reveals that, in low as well as high frequency range, the phase velocities of quasi P_1, P_2 and S_1 waves get

Table 4
Elastic coefficients for non-piezoelectric porous material.

$e_{15} = e_{31} = e_{33} = \zeta_{15} = \zeta_{31} = \zeta_{33} = e_3^* = \tilde{\zeta}_3 = \xi_{11} = \xi_{33} = \xi_{11}^* = \xi_{33}^* = A_{11} = A_{33} = 0$
Rest of the values are same as in Table 1

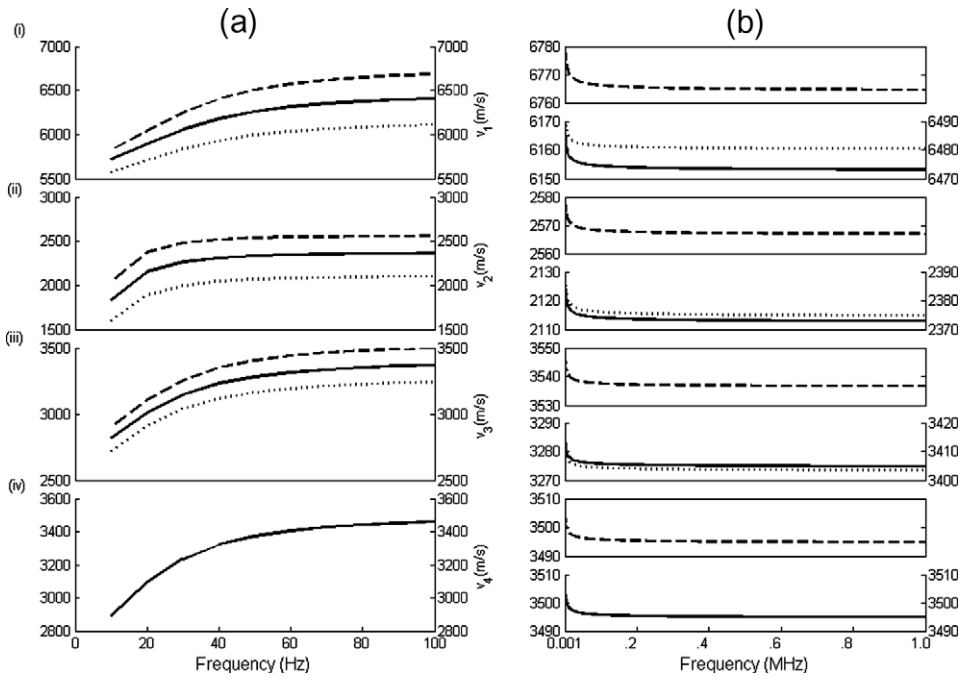

Fig. 1. Variation of phase velocity with frequency. (a) Low frequency range (LFR); (b) high frequency range (HFR): (i) P_1 wave, (ii) P_2 wave, (iii) S_1 wave, (iv) S_2 wave; Set 1 (dotted curve, left scale), Set 3 (dashed curve, left scale), Set 2 (solid curve, right scale), here $\theta = 30^\circ, \varphi = 60^\circ, f = 0.2$.

affected (increased) due to effect of piezoelectricity for artificially polarized piezoelectric material $BaTiO_3$ with epoxy. This observation agrees well with the earlier established results. However, the phase velocities of quasi P_1, P_2 and S_1 waves get decreased due to piezoelectric interaction when data are taken according to Table 1 (see dotted and solid curves). The choice of the piezoelectric and dielectric constants for the fluid-phase of the porous piezoelectric materials thus plays a significant role. The effect of piezoelectricity on the phase velocity of S_2 wave is null. The effect of piezoelectric coupling in case of $BaTiO_3$ is considerably high in comparison to that observed in a Quartz crystal (Nayfeh and Chien, 1992).

Fig. 2(a) and (b) depicts the variation of phase velocity of P_1, P_2, S_1 and S_2 waves with pore volume fraction in LFR and HFR, respectively. It is observed that in LFR, the phase velocity of all the waves decreases rapidly with porosity while it increases monotonically with porosity in HFR. The decrease in phase velocity with increase of porosity can be well described on the basis of

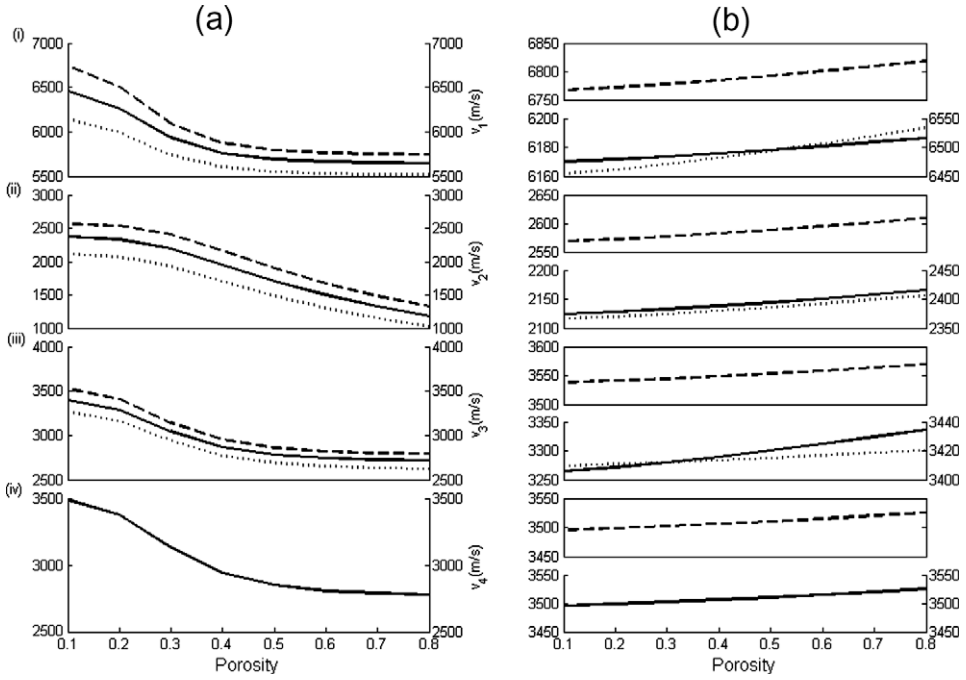

Fig. 2. Variation of phase velocity with porosity. (a) Low frequency range; (b) high frequency range: (i) P_1 wave, (ii) P_2 wave, (iii) S_1 wave, (iv) S_2 wave; Set 1 (dotted curve, left scale), Set 3 (dashed curve, left scale), Set 2 (solid curve, right scale), here $\theta = 30^\circ, \varphi = 60^\circ, \upsilon = 50$ Hz (LFR) and $\upsilon = 10,000$ Hz (HFR).

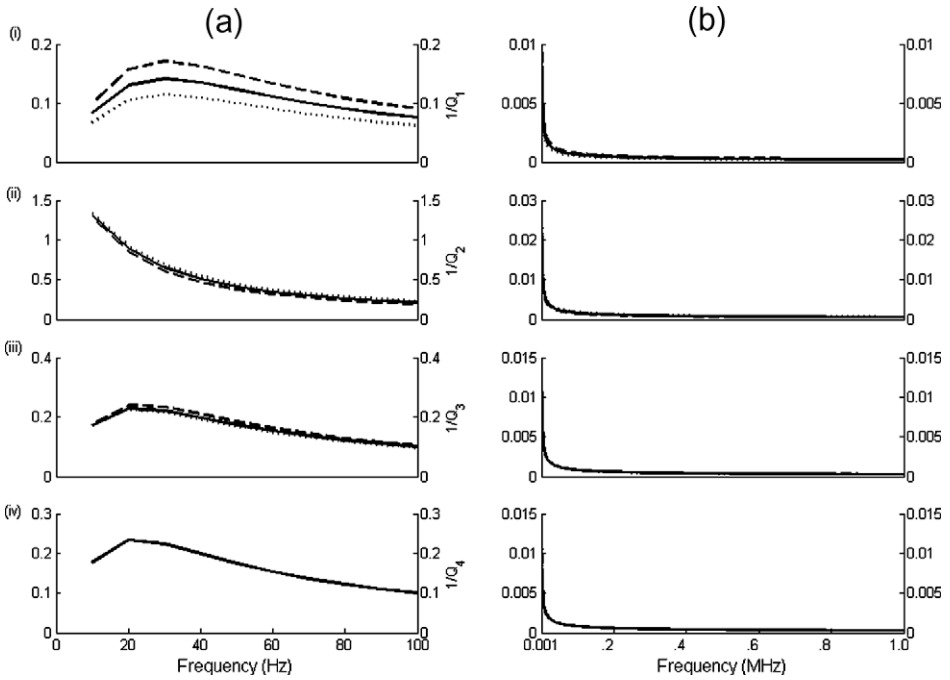

Fig. 3. Variation of attenuation quality factor with frequency. (a) Low frequency range; (b) high frequency range: (i) P_1 wave, (ii) P_2 wave, (iii) S_1 wave, (iv) S_2 wave; Set 1 (dotted curve, left scale), Set 3 (dashed curve, left scale), Set 2 (solid curve, right scale), here $\theta = 30^\circ, \varphi = 60^\circ, f = 0.2$.

percolation theory (Craciun et al., 1998). In percolation theory, a geometric phase transition occurs in the percolation system when the medium becomes disconnected due to progressive dilution, similarly to what happens in magnetic systems when the magnetization suddenly disappears at the critical temperature. Examination of Fig. 2(a) (i), (iii) and (iv) reveals that the velocities of P_1, S_1 and S_2 waves decrease slowly when the porosity is greater than 50%. It is also observed that the behavior of variation of phase velocity with porosity does not change due to the effect of piezoelectricity (see dotted, solid and dashed curves).

Next, we study the effects of frequency and the porosity on the attenuation quality factor Q_j^{-1}, $j = 1, 2, 3, 4$. Here $j = 1$ corresponds to quasi P_1 wave. Similarly indices 2, 3 and 4 correspond to quasi P_2, S_1 and S_2, waves, respectively. The attenuation is mainly contributed by viscosity losses due to the friction at the solid–liquid contact. The variation of attenuation quality factors with frequency

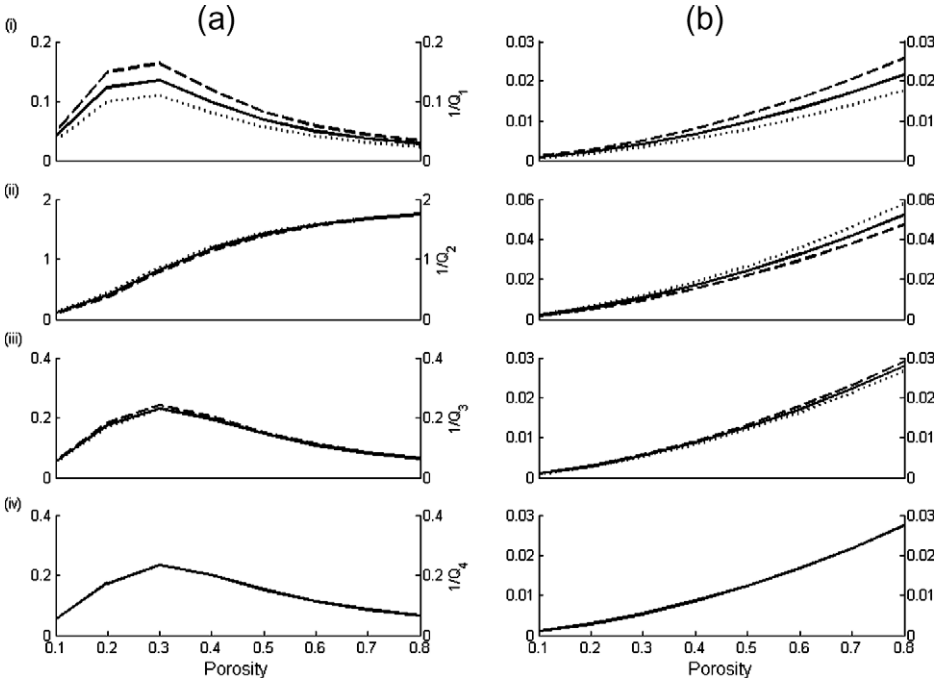

Fig. 4. Variation of attenuation quality factor with porosity. (a) Low frequency range; (b) high frequency range: (i) P_1 wave, (ii) P_2 wave, (iii) S_1 wave, (iv) S_2 wave; Set 1 (dotted curve, left scale), Set 3 (dashed curve, left scale), Set 2 (solid curve, right scale), here $\theta = 30^\circ, \varphi = 60^\circ, \upsilon = 50$ Hz (LFR) and $\upsilon = 10,000$ Hz (HFR).

is shown in Fig. 3(a) and (b) in LFR and HFR, respectively. It is observed that attenuation quality factors $1/Q_1$, $1/Q_3$ and $1/Q_4$, corresponding to P_1 wave, S_1 wave and S_2 waves, first increase with frequency in LFR and attain respective local maxima at frequency = 30 Hz and then these decrease. No specific reason is found to explain this observation. Fig. 3(a) (ii) shows that the attenuation quality factor corresponding to P_2 wave decreases monotonically with frequency in LFR. In case of HFR, it is observed from Fig. 3(b) that the quality factors corresponding to all the four waves decrease slowly and become constant after certain critical high frequency. Comparison of solid and dashed curves shows that the attenuation quality factor of P_1 wave increases when piezoelectric effects are included according to Table 2. The attenuation quality factors of other three waves remain almost unaffected due to the effect of piezoelectric interaction. The piezoelectric interaction does not affect, considerably, the attenuation of the waves in HFR.

The effect of porosity on attenuation quality factors is observed in Fig. 4. In the case of LFR, the attenuations of P_1, S_1 and S_2 waves first increase and then decrease with porosity while that of P_2 wave increases with porosity (see Fig. 4(a) (ii)). The behavior of all P_1, P_2, S_1 and S_2 waves with frequency and porosity is alike. Fig. 4(b) shows that the attenuation of all the four waves increases with porosity. It is observed the attenuation in the porous sample with high porosity is almost five times higher than in dense sample, i.e. with low value of porosity. It may be due to scattering from the geometric disorder in the sample rather than with sound absorption mechanisms in the ceramics. Comparison of dotted and solid curves reveals that, in LFR and in HFR as well, the attenuation of P_1 wave decreases when piezoelectric effects are included while that of P_2 wave increases slightly for the propagation direction $(\theta = 30^\circ, \varphi = 60^\circ)$. However, the attenuation of P_1 wave increases while that of P_2 wave decreases slightly when data are taken as shown in Table 2 (see dashed and solid curves). The effects of piezoelectric interaction on the attenuation of S_1 and S_2 waves are negligible for the permissible range of porosity.

3.2. Slowness curves, velocity curves and attenuation curves

In this section, the variation of slowness, phase velocity and the attenuation of waves propagating in the medium with the direction of propagation (θ) are studied.

Fig. 5(a) and (b) shows the slowness curves of quasi P_1, P_2, S_1 and S_2 waves for the data given in Set 1 and Set 3, respectively. The innermost curve corresponds to quasi P_1 wave and outermost curve represents that of quasi P_2 wave while other two curves correspond to quasi S_1 and quasi S_2 waves. The fact that slowness curves of S_1 and S_2 waves are not coinciding, reveals the effect of anisotropy. The slowness curve corresponding to S_2 wave is a circle which signifies a case of partial factorization that decouples the horizontally polarized quasi S_2 wave. The other three modes are coupled and polarized in the sagittal plane $\varphi = 60^\circ$. Fig. 5(a) shows that the two shear waves are degenerated along one unique propagation direction $(\theta = 0\text{—}180^\circ)$ while these waves are degenerated along three propagation directions, i.e. $\theta = 0\text{—}180^\circ$, $\theta = 30\text{—}210^\circ$ and $\theta = 150\text{—}330^\circ$, when data given in Set 3 is considered (Fig. 5(b)). This is an important characteristic because in any linear system, degenerate waves may be combined in any arbitrary manner to produce a wide variety of polarization.

To study the effects of anisotropy, the constants c_{13} and c_{33}, as given in Table 5, are changed and Fig. 6 shows that the only slowness curve corresponding to S_2 wave remain circular while those of other waves get deviated from their respective shape. The degree of deviation depends on the anisotropy. It is observed that the direction of degeneracy of S waves remain same in this case but curve corresponding to S_1 wave get bulges out which reveals that anisotropy factor (i.e. ratio of square of velocity of two waves) is greater than 1.

To study the effects of piezoelectric interaction on the wave propagation, the piezoelectric constants are allowed to vary, as specified in Tables 6 and 7. When the value of e_{15} is changed only (Table 6) the slowness curves show a significant variation, as evident from Fig. 7. Next is the case when both e_{15} and e_{33} are changed, as mentioned in Table 7 and shown in Fig. 8. Comparison of Fig. 8 with Figs. 7 and 5 shows that the variations in the value of the piezoelectric constants affect the slowness of the waves quite considerably. However, it is pertinent to mention here that these observations are made in reference to the model considered here and the particular values of the different coefficients therein.

Table 5
Elastic constants, piezoelectric constants and dielectric coefficients for PPM.

$c_{13} = 80.94$ GPa, $c_{33} = 105.5$ GPa
Rest of the values are same as in Table 1

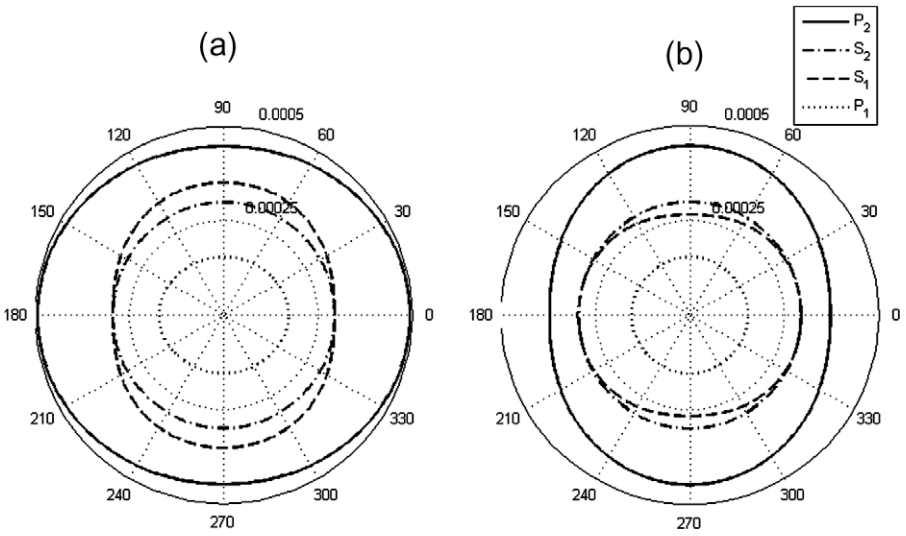

Fig. 5. Slowness curves of P_1, P_2, S_1 and S_2 waves. (a) Set 1, (b) Set 3, here $\varphi = 60^\circ, \upsilon = 50$ Hz, $f = 0.2$.

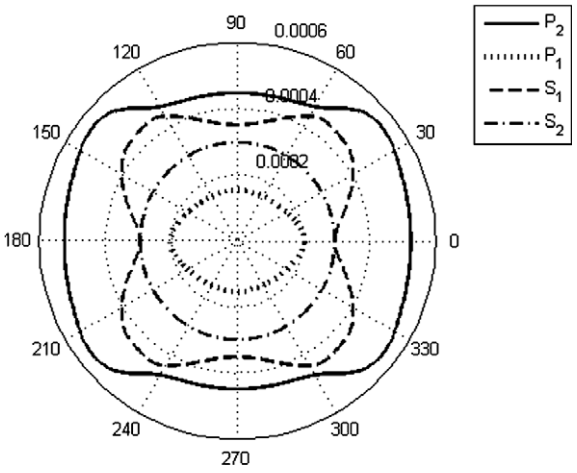

Fig. 6. Slowness curves of $P_1,\ P_2,\ S_1$ and S_2 waves corresponding for Table 5, here $\varphi = 60^\circ, \upsilon = 50$ Hz, $f = 0.2$.

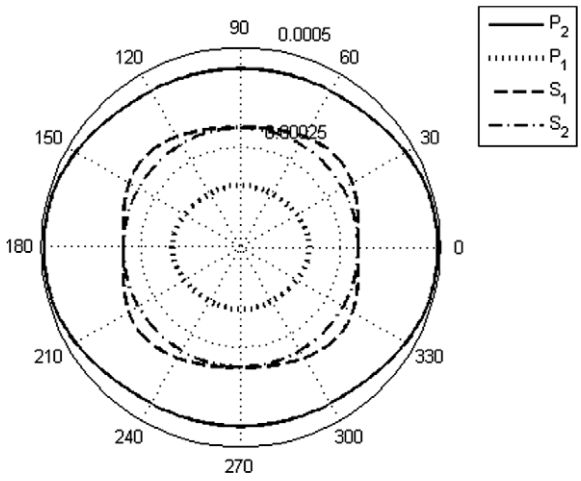

Fig. 8. Slowness curves of $P_1,\ P_2,\ S_1$ and S_2 waves corresponding for Table 7, here $\varphi = 60^\circ, \upsilon = 50$ Hz, $f = 0.2$.

Table 6
Elastic constants, piezoelectric constants and dielectric coefficients for PPM.

$e_{15} = 7.4$ C/m^2 Rest of the values are same as in Table 1

Table 8
Elastic constants, piezoelectric constants and dielectric coefficients for PPM.

$\xi_{11} = 3.8$ nC/Vm, $\xi_{33} = 14.1$ nC/Vm Rest of the values are same as in Table 1

Table 7
Elastic constants, piezoelectric constants and dielectric coefficients for PPM.

$e_{15} = 7.4$ C/m^2, $e_{33} = 22.4$ C/m^2 Rest of the values are same as in Table 1

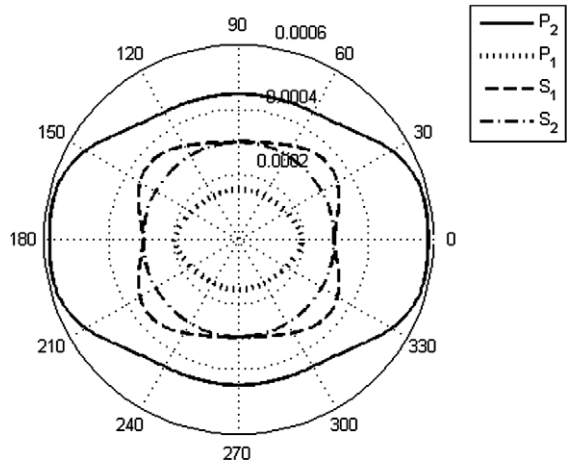

Fig. 7. Slowness curves of $P_1,\ P_2,\ S_1$ and S_2 waves corresponding for Table 6, here $\varphi = 60^\circ, \upsilon = 50$ Hz, $f = 0.2$.

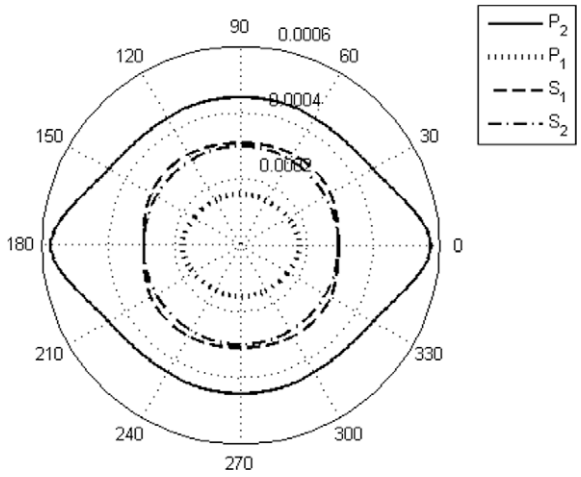

Fig. 9. Slowness curves of $P_1,\ P_2,\ S_1$ and S_2 waves corresponding for Table 8, here $\varphi = 60^\circ, \upsilon = 50$ Hz, $f = 0.2$.

To observe the effect of dielectric constants on the slowness curves, the numerical results, for the value of coefficients presented in Table 8, are shown in Fig. 9. With the variation of dielectric constants, the P_2 wave is affected more in comparison with other waves. It may be an interesting feature for further investigation that even for anisotropic PPM, with low value of dielectric constant ξ_{11}, the second kind of P wave, i.e. P_2 wave, has the tendency of decoupling for all directions except the range $0^\circ < \theta < 30^\circ, 330^\circ < \theta < 360^\circ$.

The variation of polarization skewing angle of P_1 wave (γ_1), P_2 wave (γ_2), S_1 wave (γ_3) and S_2 wave (γ_4) with the propagation direction (θ) in the sagittal plane $\varphi = 60^\circ$ is also studied and is shown in Fig. 10. The results computed corresponding for the data given in Set 1 and Set 3 are shown in Fig. 10(a) and (b), respectively. The skewing angle associated with quasi-longitudinal waves is smaller in comparison to quasi shear waves. It is also observed that the smallest skewing angle is associated with fastest wave, i.e. P_1 wave. Fig. 10(a) shows that two directions for possible propagation of pure modes can be identified corresponding to the quasi-longitudinal waves when data are taken as per Table 1. However, four directions for possible propagation of pure modes can be identified, corresponding to quasi-longitudinal waves, when computation is done for the data Set 3 (Fig. 10(b)). It is also observed that S_2 wave is polarized orthogonal to all direction of propagation in the

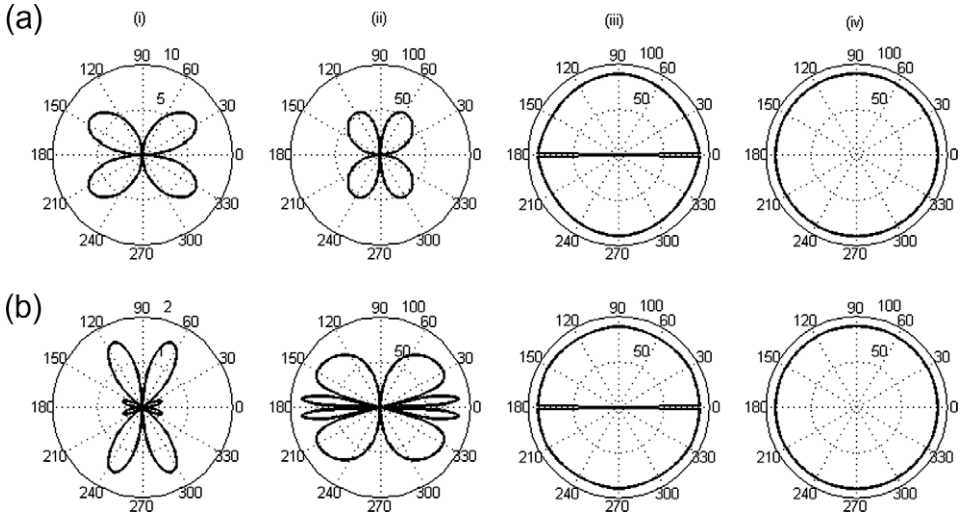

Fig. 10. Polarization skewing angle curves of $P_1,\ P_2,\ S_1$ and S_2 waves for propagation in the plane $\varphi = 60^\circ$. (a) Set 1, (b) Set 3; (i) P_1 wave, (ii) P_2 wave, (iii) S_1 wave, (iv) S_2 wave, here $\upsilon = 50$ Hz, $f = 0.2$.

sagittal plane $\varphi = 60^\circ$ which signifies the existence of pure mode for all propagation direction in x_1–x_3 plane.

Fig. 11(a) and (b) depicts the variation of angle between the polarization direction of different pair of waves with the propagation direction (θ) in the plane $\varphi = 60^\circ$ for the data given in Set 1 and Set 3, respectively. The angle between the polarization direction of *ith* and *jth* wave is denoted by θ_{ij}. Here $j = 1$ corresponds to P_1 wave. Similarly $j = 2$, 3 and 4 corresponds to $P_2,\ S_1$ and S_2 wave. It is observed that for the propagation in x_1–x_3 plane, S_2 wave is decoupled in all the directions from other three waves, i.e. $P_1,\ P_2$ and S_1 waves and polarized orthogonal to the plane containing the polarization vectors of these three waves.

To study the dependence of phase velocity on the propagation direction (θ), which holds for anisotropic materials, the velocity curves of quasi $P_1,\ P_2,\ S_1$ and S_2 waves in the plane $\varphi = 60^\circ$ and in LFR are shown in Fig. 12. The results have also been calculated by varying azimuthal angle φ but it has been found that wave velocities do not vary with φ, as expected in case of transverse isotropic material. This is one of the checks imposed for the verification of numerical computation of the results. The phase velocity of P_1 wave is affected by variation in θ only by a very small amount but anisotropy effects on the velocity of P_2 and S_1 wave is noticeable. The phase velocity of S_2 wave is independent on phase direction effectively, as expected. Comparison between the dotted, solid and dashed curves presents the effects of piezoelectric–elastic interaction in anisotropic porous materials. The phase velocities of $P_1,\ P_2$ and S_1 waves get affected due to piezoelectric interaction but that of S_2 wave remain almost unaffected (see solid, dotted and dashed curves). Comparison of the solid curves with the dotted and the dashed curves reveals that the three curves in case of P_1 and P_2 waves coincide in the region where $60^\circ \leqslant \theta \leqslant 120^\circ$ and $240^\circ \leqslant \theta \leqslant 300^\circ$. For S_1 wave, these curves coincide along the phase directions $\theta = 0$—180° implying that the phase velocity of S_1 wave is affected most by piezoelectric interaction in the range $30^\circ < \theta < 150^\circ$ and its symmetric counterpart. It is a noticeable fact that the phase velocity of S_2 wave remains unaltered in these cases. The behavior of variation of phase velocity of respective waves with θ in case of HFR is found not much different from

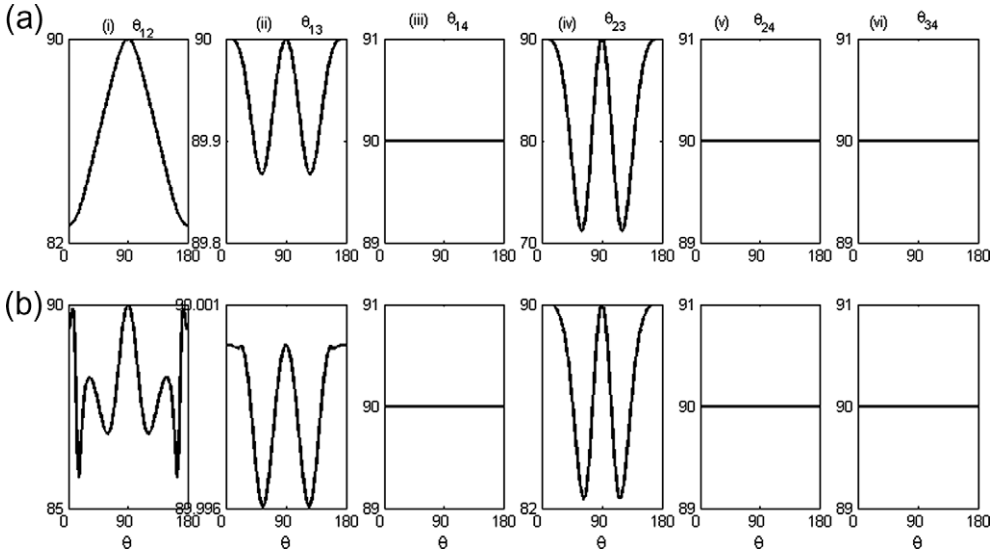

Fig. 11. Variation of angle (θ_{ij}) between the polarization vectors with direction of propagation (θ) for propagation in the plane $\varphi = 60^\circ$. (a) Set 1, (b) Set 3, here $\upsilon = 50$ Hz, $f = 0.2$.

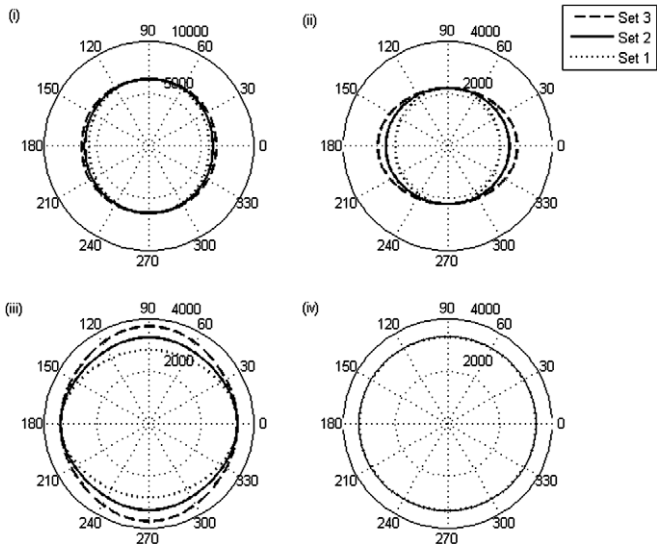

Fig. 12. Velocity curves of quasi P_1, P_2, S_1 and S_2 waves. (i) P_1 wave, (ii) P_2 wave, (iii) S_1 wave, (iv) S_2 wave, here $\varphi = 60^\circ, \upsilon = 50$ Hz, $f = 0.2$.

LFR with the only exception of increase in the velocities of respective waves in case of HFR.

To study the effects of anisotropy, the variation of phase velocities of four different waves with θ is considered for the following data sets:

Set4 = The values of the elastic and dynamic coefficients as given in Table 9 for isotropic, non-piezoelectric porous material; represented by solid curves.
Set5 = The values of the elastic, piezoelectric, dielectric and dynamic coefficients as given in Tables 5 and 3 for PPM; represented by dashed curves.

Comparison of dashed curve (Fig. 13) with the dotted curve reveals that the variation in the value of elastic constants c_{13} and c_{33} does not affect the velocity of S_2 wave. It is observed that the velocity of S_1 wave is maximum along the direction $\theta = 0$—180°, i.e. along the axis of symmetry. The velocity curve of the P_1 wave for the above mentioned variation in constants depicts that significant changes occur for the range $0^\circ \leqslant \theta \leqslant 30^\circ$ and $330^\circ \leqslant \theta \leqslant 360^\circ$. Similarly P_2 wave changes its behavior in the region $30^\circ \leqslant \theta \leqslant 60^\circ$ and its symmetric counterparts in other three quadrants. The solid curve shows the velocity curves of respective waves for the case of non-piezoelectric isotropic porous material. In this case, the velocity curve of S_1 and S_2 waves coincides, as expected. It is noticed that the phase velocities of P_1, P_2 and S_1 waves decreases when piezoelectric effect or anisotropic effect or both are included. It is observed that the phase velocity of P_1 and P_2 waves remain unaffected along the direction $\theta = 90$—270° in all the three discussed cases while that of S_1 wave remain same along the direction$\theta = 0$—180°. The graphs shown in this figure have been computed in LFR. However, results have also been computed for HFR but found not to be significantly different from the present ones, so we omit the repetitions.

Table 9
Elastic and dynamic coefficients for isotropic non-piezoelectric porous material.

$c_{13} = c_{12},\ c_{33} = c_{11},\ c_{66} = c_{44},\ m_{33} = m_{11}$
$[\rho_{11}]_{33} = [\rho_{11}]_{11},\ [\rho_{12}]_{33} = [\rho_{12}]_{11},\ [\rho_{22}]_{33} = [\rho_{22}]_{11}$
$\chi_{33} = \chi_{11}$
Rest of the values are same as given in Tables 4 and 3.

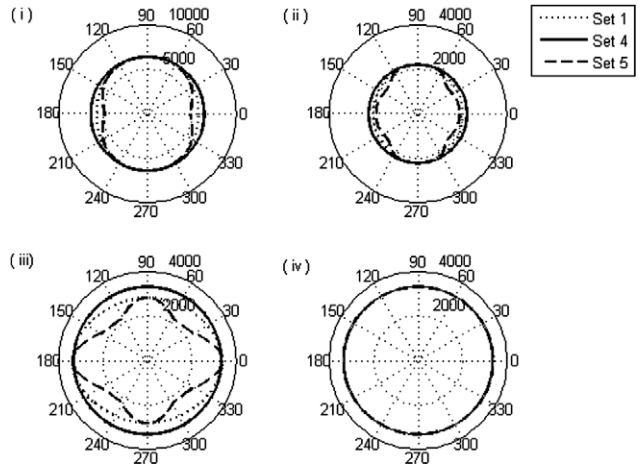

Fig. 13. Velocity curves of quasi P_1, P_2, S_1 and S_2 waves. (i) P_1 wave, (ii) P_2 wave, (iii) S_1 wave, (iv) S_2 wave, here $\varphi = 60^\circ, \upsilon = 50$ Hz, $f = 0.2$.

The dependence of attenuation quality factors of all the four waves on the phase direction and piezoelectric interaction in the LFR is depicted in Fig. 14. The solid curve depicts the variation of attenuation quality factor with phase direction when piezoelectric interaction is absent. The dotted and dashed curves show the variation of attenuation quality factors with the phase direction corresponding to the data given in Set 1 and Set 3, respectively. The attenuation of S_1 is affected most in the region $\theta = 10$—70° and its symmetric counterparts. The effect of piezoelectric interaction on the attenuation of S_2 is null. Comparison of dotted curve with the dashed and the solid curve reveals that the change in the behavior of attenuation curves of P_1 and P_2 wave is maximum along the direction $\theta = 0$—180° and is nil along the direction $\theta = 90$—270°.

To see the effects of anisotropy on the attenuation, the elastic constants c_{13} and c_{33} are changed, as prescribed in Set 5. The corresponding attenuation curves (dashed curve) for all the four waves are shown in Fig. 15. Comparison between the dashed and dotted curves clearly depicts the effects of the anisotropy. Due to change in above mentioned elastic constants, the attenuation of P_1/P_2 wave is minimum/maximum along the direction

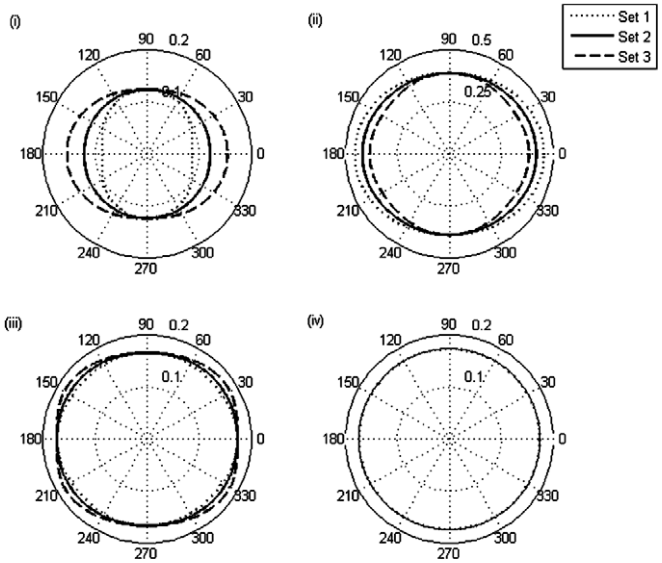

Fig. 14. Attenuation curves of quasi P_1, P_2, S_1 and S_2 waves. (i) P_1 wave, (ii) P_2 wave, (iii) S_1 wave, (iv) S_2 wave, here $\varphi = 60^\circ, \upsilon = 50$ Hz, $f = 0.2$.

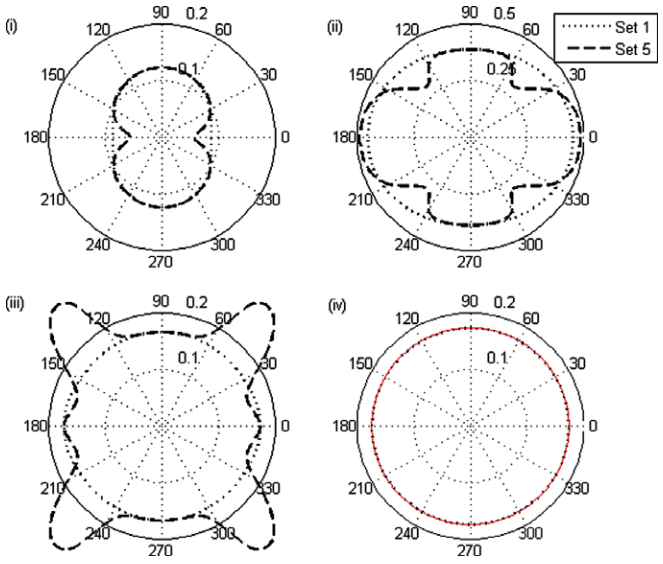

Fig. 15. Attenuation curves of quasi P_1, P_2, S_1 and S_2 waves. (i) P_1 wave, (ii) P_2 wave, (iii) S_1 wave, (iv) S_2 wave, here $\varphi = 60^\circ, \upsilon = 50$ Hz, $f = 0.2$.

$\theta = 0$–180° while that of S_1 wave is maximum along the directions $\theta = 45^\circ$, 135°, 225° and 315°. The attenuation curve of S_1 wave shows interesting behavior in the region where $0^\circ \leqslant \theta \leqslant 30^\circ$ and $330^\circ \leqslant \theta \leqslant 360^\circ$and corresponding other symmetric half. The anisotropy has no effects on the attenuation of S_2 wave. The results are also computed for the case of HFR but there is not a significant change in the behavior of variation of attenuation quality factor with θ, with the exception of decrease in the value of the attenuation in case of HFR.

4. Conclusion

In the present paper, wave propagation in porous piezoelectric material having 6 mm type symmetry is studied both analytically and numerically. The constitutive equations and dynamical equations for PPM are formulated in the paper. The four complex roots of the obtained Christoffel equation define the phase velocities of propagation and the attenuation quality factors of four stiffened quasi waves propagating in such a medium. The variation of phase velocities and attenuation quality factors of these waves with frequency, phase direction and the porosity is observed numerically in a reference of porous piezoelectric crystal $BaTiO_3$. The phase velocities of all the four waves increase with frequency in LFR but decrease in HFR. The phase velocities of all the four waves decrease with porosity in LFR which can be explained on the basis of percolation theory. The electric–elastic interaction does not affect the behavior of phase velocities with porosity. The variation pattern of attenuation quality factors and phase velocities with frequency is alike. The attenuation in the porous sample with high porosity is almost five times higher than in dense sample (with low value of porosity). It may be due to the scattering from the geometric disorder in the sample rather than with sound absorption mechanism in the ceramics. The characteristic curves including slowness curves, velocity curves, and the attenuation curves are also obtained for all the four waves. The slowness curve corresponding to S_2 wave is a perfect circle which signifies a case of decoupling of horizontally polarized S_2 wave. The other three modes are coupled and polarized in the sagittal plane. The shapes of characteristic curves of all the waves except S_2 wave get deviated with change in elastic constantsc_{13} and c_{33}. With the variation of dielectric constants, the P_2 wave is affected more in comparison to other waves. It may be an interesting feature for further investigation that even for anisotropic PPM, with low value of dielectric constant, the second kind of P wave, i.e. P_2, has the tendency of decoupling for all direction except a particular range. The anisotropy effects on the velocity of S_1 wave are noticeable in comparison to P_1 and P_2 waves. The phase velocity of S_2 wave is independent of phase direction.

Appendix A

$$
\begin{aligned}
&\mathbf{A}_1 = \mathbf{K}_1 h - \bar{\boldsymbol{\rho}}_{11},\ \ \mathbf{A}_2 = \mathbf{K}_2 h - \bar{\boldsymbol{\rho}}_{12},\\
&\mathbf{A}_3 = \mathbf{K}_3 h - \bar{\boldsymbol{\rho}}_{12},\ \ \mathbf{A}_4 = k_4 \mathbf{n}^{\mathbf{T}}\mathbf{n} h - \bar{\boldsymbol{\rho}}_{22},\\
&\bar{\boldsymbol{\rho}}_{11} = \boldsymbol{\rho}_{11} + (\imath/\omega)\mathbf{b},\ \ \bar{\boldsymbol{\rho}}_{22} = \boldsymbol{\rho}_{22} + (\imath/\omega)\mathbf{b},\\
&\bar{\boldsymbol{\rho}}_{12} = \boldsymbol{\rho}_{12} - (\imath/\omega)\mathbf{b},\\
&h = R/(\rho v^2),\\
&\mathbf{K}_1 = \mathbf{P} + \mathbf{e}^T \otimes \mathbf{r} + \boldsymbol{\zeta}^T \otimes \mathbf{b}^*,\quad \mathbf{K}_2 = \mathbf{M}\mathbf{n}^T\mathbf{n} + \mathbf{e}^T \otimes \mathbf{t} + \boldsymbol{\zeta}^T \otimes \mathbf{z},\\
&\mathbf{K}_3 = \mathbf{n}^T\mathbf{n}\mathbf{M} + (\mathbf{n}')^T \otimes \mathbf{r} + (\mathbf{n}^*)^T \otimes \mathbf{b}^*,\\
&k_4 = 1 + \tilde{\zeta}_3 n_3[e_3^* n_3/a - \xi^*(\tilde{\zeta}_3 n_3 - e_3^* n_3 \xi/a)/(a^2 - \xi\xi^*)]\\
&\qquad + e_3^* n_3 a(\tilde{\zeta}_3 n_3 - e_3^* n_3 \xi/a)/(a^2 - \xi\xi^*),\\
&\mathbf{e} = [e_1 \quad e_2 \quad e_3],\ \ \boldsymbol{\zeta} = [\zeta_1 \quad \zeta_2 \quad \zeta_3],\\
&\mathbf{n}' = [n_1' \quad n_2' \quad n_3'],\ \ \mathbf{n}^* = [n_1^* \quad n_2^* \quad n_3^*],\\
&\mathbf{n} = [n_1 \quad n_2 \quad n_3],\ \ \mathbf{r} = [r_1 \quad r_2 \quad r_3],\\
&\mathbf{b}^* = [b_1^* \quad b_2^* \quad b_3^*],\ \ \mathbf{t} = [t_1 \quad t_2 \quad t_3],\\
&\mathbf{z} = [z_1 \quad z_2 \quad z_3],\ \ \mathbf{M} = [m_{ij}]_{3\times 3},\quad \mathbf{P} = [P_{ij}]_{3\times 3}.
\end{aligned}
\tag{A.1}
$$

where superscript T denotes the transpose of vector/matrix.

$$
\begin{aligned}
&e_1 = (e_{15} + e_{31}) n_1 n_3,\\
&e_2 = (e_{15} + e_{31}) n_1 n_3,\\
&e_3 = e_{15} n_1^2 + e_{15} n_2^2 + e_{33} n_3^2,\\
&\zeta_1 = (\zeta_{15} + \zeta_{31}) n_1 n_3,\\
&\zeta_2 = (\zeta_{15} + \zeta_{31}) n_1 n_3,\\
&\zeta_3 = \zeta_{15} n_1^2 + \zeta_{15} n_2^2 + \zeta_{33} n_3^2,\\
&n_k' = \tilde{\zeta}_3 n_3 n_k,\\
&n_k^* = e_3^* n_3 n_k,\\
&\xi = \xi_{11} n_1^2 + \xi_{11} n_2^2 + \xi_{33} n_3^2,\\
&\xi^* = \xi_{11}^* n_1^2 + \xi_{11}^* n_2^2 + \xi_{33}^* n_3^2,\\
&a = A_{11} n_1^2 + A_{11} n_2^2 + A_{33} n_3^2,\\
&\mathbf{r} = \frac{1}{a}\boldsymbol{\zeta} - \frac{\xi^*}{a^2 - \xi\xi^*}\left(\mathbf{e} - \frac{\xi}{a}\boldsymbol{\zeta}\right),\\
&\mathbf{b}^* = \frac{a}{a^2 - \xi\xi^*}\left(\mathbf{e} - \frac{\xi}{a}\boldsymbol{\zeta}\right),\\
&\mathbf{t} = \frac{1}{a}\mathbf{n}^* - \frac{\xi^*}{a^2 - \xi\xi^*}\left(\mathbf{n}' - \frac{\xi}{a}\mathbf{n}^*\right),\\
&\mathbf{z} = \frac{a}{a^2 - \xi\xi^*}\left(\mathbf{n}' - \frac{\xi}{a}\mathbf{n}^*\right),\\
&P_{11} = c_{11} n_1^2 + c_{66} n_2^2 + c_{44} n_3^2,\\
&P_{12} = c_{12} n_1 n_2 + c_{66} n_1 n_2,\\
&P_{13} = c_{13} n_1 n_3 + c_{55} n_1 n_3,\\
&P_{22} = c_{66} n_1^2 + c_{22} n_2^2 + c_{44} n_3^2,\\
&P_{23} = c_{44} n_2 n_3 + c_{23} n_2 n_3,\\
&P_{33} = c_{66} n_1^2 + c_{44} n_2^2 + c_{33} n_3^2,\\
&c_{ij} = c_{ij}/R,\ \ e_{ij} = e_{ij}/R,\ \ \zeta_{ij} = \zeta_{ij}/R,\ \ m_{ij} = m_{ij}/R,\\
&\xi_{ij} = \xi_{ij}/R,\ \ \xi_{ij}^* = \xi_{ij}^*/R,\ \ A_{ij} = A_{ij}/R,\\
&e_k^* = e_k^*/R,\ \ \tilde{\zeta}_k = \tilde{\zeta}_k/R,\ \ b_{ij} = b_{ij}/\rho,\\
&\boldsymbol{\rho}_{11} = \boldsymbol{\rho}_{11}/\rho,\ \ \boldsymbol{\rho}_{12} = \boldsymbol{\rho}_{12}/\rho,\ \ \boldsymbol{\rho}_{22} = \boldsymbol{\rho}_{22}/\rho.
\end{aligned}
\tag{A.2}
$$

Appendix B

$$
\begin{aligned}
&x = c_1 h + c_2,\\
&\mathbf{B} = \mathbf{K}_1 - \frac{\mathbf{X}_2}{c_1},\\
&\mathbf{C} = -\bar{\boldsymbol{\rho}}_{11} - \left(\mathbf{X}_3 - \frac{c_2}{c_1}\mathbf{X}_2\right)\Big/ c_1,\\
&\mathbf{D} = -\mathbf{X}_4 + \left(\mathbf{X}_3 - \frac{c_2}{c_1}\mathbf{X}_2\right)\frac{c_2}{c_1},
\end{aligned}
\tag{B.1}
$$

where

$$
\begin{aligned}
&\mathbf{X}_2 = -\mathbf{K}_2\mathbf{F}\bar{\boldsymbol{\rho}}_{12} + \mathbf{K}_2\mathbf{G}\mathbf{K}_3 - \bar{\boldsymbol{\rho}}_{12}\mathbf{F}\mathbf{K}_3,\\
&\mathbf{X}_3 = -\mathbf{K}_2\mathbf{G}\bar{\boldsymbol{\rho}}_{12} + \bar{\boldsymbol{\rho}}_{12}\mathbf{F}\bar{\boldsymbol{\rho}}_{12} - \bar{\boldsymbol{\rho}}_{12}\mathbf{G}\mathbf{K}_3,\\
&\mathbf{X}_4 = \bar{\boldsymbol{\rho}}_{12}\mathbf{G}\bar{\boldsymbol{\rho}}_{12},\\
&c_1 = k_4 n_1^2 d_1 + k_4 n_2^2 d_4 + k_4 n_3^2 d_6,\\
&c_2 = -[\bar{\boldsymbol{\rho}}_{22}]_{11} d_4,\\
&G = \begin{bmatrix} d_1 & 0 & 0\\ 0 & d_4 & 0\\ 0 & 0 & d_6 \end{bmatrix},\\
&d_1 = [\bar{\boldsymbol{\rho}}_{22}]_{11}[\bar{\boldsymbol{\rho}}_{\mathbf{22}}]_{33},\\
&d_4 = [\bar{\boldsymbol{\rho}}_{22}]_{11}[\bar{\boldsymbol{\rho}}_{\mathbf{22}}]_{33},\\
&d_6 = [\bar{\boldsymbol{\rho}}_{22}]_{11}[\bar{\boldsymbol{\rho}}_{\mathbf{22}}]_{11},\\
&[\mathbf{F}]_{11} = (-[\bar{\boldsymbol{\rho}}_{22}]_{33} n_2^2 - [\bar{\rho}_{22}]_{11} n_3^2) k_4\\
&[\mathbf{F}]_{12} = [\bar{\boldsymbol{\rho}}_{22}]_{33} n_1 n_2 k_4\\
&[\mathbf{F}]_{13} = [\bar{\boldsymbol{\rho}}_{22}]_{11} n_1 n_3 k_4\\
&[\mathbf{F}]_{22} = (-[\bar{\boldsymbol{\rho}}_{22}]_{11} n_3^2 - [\bar{\boldsymbol{\rho}}_{22}]_{33} n_1^2) k_4,\\
&[\mathbf{F}]_{23} = [\bar{\boldsymbol{\rho}}_{22}]_{11} n_2 n_3 k_4,\\
&[\mathbf{F}]_{33} = (-[\bar{\boldsymbol{\rho}}_{22}]_{11} n_1^2 - [\bar{\boldsymbol{\rho}}_{22}]_{11} n_2^2) k_4.
\end{aligned}
\tag{B.2}
$$

Appendix C

$$
\begin{aligned}
&T_1 = B_{11} y_1 + B_{12} y_6 + B_{13} y_{11},\\
&T_2 = C_{11} y_1 + C_{12} y_6 + C_{13} y_{11} + B_{11} y_2 + B_{12} y_7 + B_{13} y_{12},\\
&T_3 = C_{11} y_2 + C_{12} y_7 + C_{13} y_{12} + B_{11} y_4 + B_{12} y_9 + B_{13} y_{14},\\
&T_4 = C_{11} y_4 + C_{12} y_9 + C_{13} y_{14},\\
&T_5 = D_{11} y_1 + D_{12} y_6 + D_{13} y_{11} + B_{11} y_3 + B_{12} y_8 + B_{13} y_{13},\\
&T_6 = D_{11} y_2 + D_{12} y_7 + D_{13} y_{12} + C_{11} y_3 + C_{12} y_8\\
&\qquad + C_{13} y_{13} + B_{11} y_5 + B_{12} y_{10} + B_{13} y_{15},\\
&T_7 = D_{11} y_4 + D_{12} y_9 + D_{13} y_{14} + C_{11} y_5 + C_{12} y_{10} + C_{13} y_{15},
\end{aligned}
\tag{C.1}
$$

where

$$
\begin{aligned}
&y_1 = B_{22} B_{33} - B_{23} B_{32},\\
&y_2 = B_{22} C_{33} + C_{22} B_{33} - B_{23} C_{32} - C_{23} B_{32},\\
&y_3 = B_{22} D_{33} + D_{22} B_{33} - B_{23} D_{32} - D_{23} B_{32},\\
&y_4 = C_{22} C_{33} - C_{23} C_{32},\\
&y_5 = C_{22} D_{33} + D_{22} C_{33} - C_{23} D_{32} - D_{23} C_{32},\\
&y_6 = B_{31} B_{23} - B_{21} B_{33},\\
&y_7 = B_{31} C_{23} + C_{31} B_{23} - B_{21} C_{33} - C_{21} B_{33},\\
&y_8 = B_{21} D_{33} + D_{21} B_{33} - B_{23} D_{31} - D_{23} B_{31},\\
&y_9 = C_{21} C_{33} - C_{23} C_{31},\\
&y_{10} = C_{21} D_{33} + D_{21} C_{33} - C_{23} D_{31} - D_{23} C_{31},\\
&y_{11} = B_{21} B_{32} - B_{31} B_{22},\\
&y_{12} = B_{21} C_{32} + C_{21} B_{32} - B_{31} C_{22} - C_{31} B_{22},\\
&y_{13} = B_{21} D_{32} + D_{21} B_{32} - B_{31} D_{22} - D_{31} B_{22},\\
&y_{14} = C_{21} C_{32} - C_{22} C_{31},\\
&y_{15} = C_{21} D_{32} + D_{21} C_{32} - C_{22} D_{31} - D_{22} C_{31}.
\end{aligned}
\tag{C.2}
$$

References

Arai, T., Ayusawa, K., Sato, H., Miyata, T., Kawamura, K., Kobayashi, K., 1991. Properties of hydrophone with porous piezoelectric ceramics. Japanese Journal of Applied Physics 30, 2253–2255.

Arnau, A., 2004. Piezoelectric Transducers and Applications. Springer, New York.

Arnau, A. (Ed.), 2008. Piezoelectric Transducers and Applications. Springer, New York.

Auld, B.A., 1973. Acoustic Fields and Waves in Solids, vol. 1. Wiley, New York. Inclusive.

Auld, B.A., 1981. Wave propagation and resonance in piezoelectric materials. Journal of the Acoustic Society of America 70 (6), 1577–1585.

Banno, H., 1989a. Theoretical equations for dielectric, piezoelectric and elastic properties of flexible composite consisting of polymer and ceramic powder of two different materials. Ferroelectric 95, 111–115.

Banno, H., 1989b. Theoretical equations for dielectric, piezoelectric and elastic properties of 0–3 composite based on modified cubes model – a general solution. Japanese Journal of Applied Physics Supplementary 28 (2), 190–192.

Banno, H., 1993. Effects of porosity on dielectric, elastic and electromechanical properties of $Pb(Zr,Ti)O_3$ ceramics with open pores: a theoretical approach. Japanese Journal of Applied Physics 32, 4214–4217.

Biot, M.A., 1956. Theory of propagation of elastic waves in a fluid-saturated porous solid. I. Low frequency range. Journal of the Acoustic Society of America 28 (2), 168–178.

Biot, M.A., 1962. Mechanics of deformation and acoustic propagation in porous media. Journal of Applied Physics 33 (4), 1482–1498.

Bisegna, P., Luciano, R., 1996. Variational bounds for the overall properties of piezoelectric composites. Journal of the Mechanical and Physics of Solids 44 (4), 583–602.

Bowen, C.R., Perry, A., Lewis, A.C.F., Kara, H., 2004. Processing and properties of porous piezoelectric materials with high hydrostatic figures of merit. Journal of the European Ceramic Society 24, 541–545.

Craciun, F., Guidarelli, G., Galassi, C., Roncari, E., 1998. Elastic wave propagation in porous piezoelectric ceramics. Ultrasonic 36, 427–430.

Dong, K., Wang, X., 2007. Wave propagation characteristics in piezoelectric cylindrical laminated shells under large deformation. Composite Structures 77, 171–181.

Galassi, C., Dinescu, M., Uchino, K., Sayer, M. (Eds.), 2000. Piezoelectric Materials: Advances in Science, Technology and Applications, vol. 76. Springer, New York.

Gomez, T.E., Montero, F., 1996. Highly coupled dielectric behavior of porous ceramics embedding a polymer. Applied Physics Letters 68, 263–265.

Gomez, T.E., Elvira, L., Riera, E., 1995. Generations of slow wave to characterize air filled porous fabrics. Journal of Applied Physics 78, 2843–2845.

Gomez, T.E., Mulholland, A.J., Hayward, G., Gomatam, J., 2000. Wave propagation in 0–3/3–3 connectivity composites with complex microstructure. Ultrasonics 38, 897–907.

Gupta, R.K., Venkatesh, T.A., 2006. Electromechanical response of porous piezoelectric materials. Acta Materialia 54, 4063–4078.

Hashimoto, K.Y., Yamaguchi, M., 1986. Elastic, piezoelectric and dielectric properties of composite materials. Proceeding IEEE Ultrasonics Symposium 2, 697–702.

Hayashi, T., Sugihara, K., Okazaki, K., 1991. Processing of porous 3–3 PZT ceramics using capsule-free O2 H.P.. Japanese Journal of Applied Physics 30, 2243–2246.

Hsu, J.C., Wu, T.T., 2008. Calculations of Lamb wave band gaps and dispersions for piezoelectric phononic plates using Mindlin's theory-based plane wave expansion method. IEEE Transactions on Ultrasonics, Ferroelectrics and Frequency Control 55, 431–441.

Huang, S., Chang, J., Lu, L., Liu, F., Ye, Z., Cheng, X., 2006. Preparation and polarization of 0–3 cement based piezoelectric composites. Materials Research Bulletin 41, 291–297.

Ikeda, T., 1990. Fundamentals of Piezoelectricity. Oxford Science, Oxford University Press.

Johnson, D.L., Koplik, J., Dashen, R., 1987. Theory of dynamic permeability and tortuosity in fluid-saturated porous media. Journal of Fluid Mechanics 176, 379–402.

Katzir, S., 2006. The Beginning of Piezoelectricity – A Study in Mundane Physics, vol. 246. Springer, New York.

Khoroshun, L.P., Dorodnykh, T.I., 2003. Modeling the short-term damageability of a transversely isotropic piezoelectric material. International Applied Mechanics 39 (9), 1046–1053.

Lacour, O., Lagier, M., Sornette, D., 1994. Effect of dynamic fluid compressibility and permeability on porous piezoelectric ceramics. Journal of the Acoustic Society of America 96 (6), 3548–3557.

Li, F.M., Wang, Y.S., 2005. Study on wave localization in disordered periodic layered piezoelectric composite structures. International Journal of Solids and Structures 42, 6457–6474.

Li, F.M., Wang, Y., Hu, C., Huang, W., 2006. Wave localization in randomly disordered periodic layered piezoelectric structures. Acta Mechanica Sinica 22, 559–567.

Mesquida, A.A., Otero, J.A., Ramos, R.R., Comas, F., 1998. Wave propagation in layered piezoelectric structures. Journal of Applied Physics 83 (9), 4652–4659.

Mesquida, A.A., Ramos, R.R., Comas, F., Monsivais, G., Sirvent, R.E., 2001. Scaterring of shear horizontal piezoelectric waves in piezocomposite media. Journal of Applied Physics 89 (5), 2886–2892.

Mizumura, K., Kurihara, Y., Ohashi, H., Kumamoto, S., Okuno, K., 1991. Porous piezoelectric ceramic transducer. Japanese Journal of Applied Physics 30, 2271–2273.

Nayfeh, A.H., Chien, H.T., 1992. Wave propagation interaction with free and fluid loaded piezoelectric substrates. Journal of the Acoustic Society of America 91 (6), 3126–3135.
Nayfeh, A.H., Faidi, W., Abdelrahman, W., 1999. An approximate model for wave propagation in piezoelectric materials. 1. Laminated composites. Journal of Applied Physics 85 (4), 2337–2346.
Newnham, R.E., 2005. Properties of Materials: Anisotropy, Symmetry and Structure. Oxford Science, Oxford University Press.
Pan, E., Han, F., 2004. Green's functions for transversely isotropic piezoelectric multilayered half-spaces. Journal of Engineering Mathematics 49, 271–288.
Pan, E., Han, F., 2005. Green's functions for transversely isotropic piezoelectric functionally graded multilayered half-spaces. International Journal of Solids and Structures 42, 3207–3233.
Piazza, D., Capiani, C., Galassi, C., 2005. Piezoceramic material with anisotropic graded porosity. Journal of the European Ceramic Society 25, 3075–3078.
Piazza, D., Stoleriu, L., Mitoseriu, L., Stancu, A., Galassi, C., 2006. Characterization of porous PZT ceramics by first order reversal curves (FORC) diagrams. Journal of the European Ceramic Society 26, 2959–2962.
Praveenkumar, B., Kumar, H.H., Kharat, D.K., 2005. Characterization and microstructure of porous lead zirconate titanate ceramics. Bulletin of Materials Science 28 (5), 453–455.
Qian, Z., Jin, F., Kishimoto, K., Wang, Z., 2004a. Effect of initial stress on the propagation behavior of SH waves in multilayered piezoelectric composite structures. Sensor and Actuators A 112, 368–375.
Qian, Z., Jin, F., Wang, Z., Kishimoto, K., 2004b. Dispersion relations for SH wave propagation in periodic piezoelectric composite layered structures. International Journal of Engineering Science 42, 673–689.
Rasolofasaon, P.N.J., Zinszner, B.E., 2002. Comparison between permeability amisotropy and elastic anisotropy of reservoir rocks. Geophysics 67, 230–240.
Smith, W.A., Auld, A., 1990. Modeling 1–3 composite piezoelectrics: thickness-mode oscillations. IEEE Transaction on Ultrasonics Ferroelectrics and Frequency Control 38 (1), 40–47.
Tichy, J., Erhart, J., Kittinger, E., Fousek, J., Privatska, J., Janovec, V., 2007. Fundamentals of Piezoelectric Sensorics – Mechanical Dielectric and Thermodynamical Properties of Piezoelectric Materials. Springer, New York.
Uchino, K., 1997. Piezoelectric Actuators and Ultrasonic Motor. Kluwer Academic Publishers, Bosten.
Vashishth, A.K., Gupta, V., 2009. Vibrations of porous piezoelectric ceramic plate. Journal of Sound and Vibration 325, 781–797.
Wang, L., Yuan, F.G., 2007. Group velocity and characteristic wave curves of lamb waves in composites: modeling and experiments. Composites Science and Technology 67, 1370–1384.
Wang, Q., Chen, Q., Zhu, J., Huang, C., Darvell, B.W., Chen, Z., 2008. Effect of pore shape and porosity on the properties of porous LNKN ceramics as bone substitutes. Materials Chemistry and Physics 109, 488–491.
Xia, Z., Ma, S., Qui, X., Wu, Y., Wang, F., 2003. Influence of porosity on the stability of charge and piezoelectricity for porous polytetrafluoroethylene film electrets. Journal of Electrostatics 59, 57–69.
Yang, J., 2005. An Introduction to the Theory of Piezoelectricity. Springer, New York.
Zakharenko, A.A., 2007. New solutions of shear waves in piezoelectric cubic crystals. Journal of Zhejiang University Science A 8 (4), 669–674.
Zeng, T., Dong, X.L., Mao, C.L., Chen, S.T., Chen, H., 2006a. Preparation and properties of porous PMN-PZT ceramics doped with strontium. Materials Science and Engineering B 135, 50–54.
Zeng, T., Dong, X.L., Chen, H., Wang, Y.L., 2006b. The effects of sintering behavior on piezoelectric properties of porous PZT ceramics for hydrophone application. Material Science and Engineering B 131, 181–185.
Zeng, T., Dong, X.L., Mao, C.L., Zhou, Z.Y., Yang, H., 2007. Effects of pore shape and porosity on the properties of porous PZT 95/5 ceramics. Journal of the European Ceramic Society 27, 2025–2029.
Zhang, H.L., Li, J.F., Zhang, B.P., 2007. Microstructure and electrical properties of porous PZT ceramics derived from different pore-forming agents. Acta Materialia 55, 171–181.
Zinchuk, L.P., Podlipenets, A.N., 2000. Propagation of shear waves in piezoelectric superlattice-substrate structures. Journal of Mathematical Sciences 101 (6), 3688–3693.
Zinchuk, L.P., Podlipenets, A.N., 2001. Dispersion equations for Rayleigh waves in a piezoelectric periodically layered structure. Journal of Mathematical Sciences 103 (3), 398–403.